Cellulose
https://doi.org/10.1007/s10570-022-04424-w

ORIGINAL RESEARCH

Quantum-efficiency enhancement and mechanical responsiveness of solid-state photoluminescent flexible materials containing uniaxial cellulose nanocrystal arrays

Siyuan Liu · Zhenxu Shi · Xuhong Wang · Yanbin Gong · Xijun Li · Xin Jia · Lin Gan · Jin Huang

Received: 16 June 2021 / Accepted: 4 January 2022

Abstract Assembling cellulose nanocrystals (CNCs) can induce solid-state photoluminescence based on Stokes scattering. Such photoluminescent materials are free of photo-quenching and show great potential in optical applications, whereas poor flexibility of assembled CNC arrays limits their applications. Here, a binary co-assembly of 1D nanoparticles and long-chain polymers was explored to produce the uniaxial CNC arrays into transparent poly(vinyl alcohol) (PVA) membranes, which enhanced the mechanical properties, especially ductility. Besides, the CNC assembly was controlled by adjusting the mass ratio between CNCs and PVA. The result indicated that co-assembling with PVA could improve the uniaxial orientation of CNC arrays, which played a crucial role in enhancing the emission quantum efficiency (EQE). Stretching the PVA/CNC membrane could further induce an enhancement in EQE together with a blue shift in excitation wavelength. The mechanism study on stimulation-response suggested that the EQE enhancement and blue shift came from the change in uniaxial orientation degree and periodicity of the CNC assembly, respectively. Since the stimulation-responsive enhancement in EQE (from *ca*. 40 to 60%) can even be observed by naked eyes, we

Siyuan Liu and Zhenxu Shi has contributed equally to this work.

Supplementary Information The online version contains supplementary material available at https://doi.org/10.1007/s10570-022-04424-w.

S. Liu · Z. Shi · X. Wang · L. Gan (✉) · J. Huang (✉)
School of Chemistry and Chemical Engineering, Chongqing Key Laboratory of Soft-Matter Material Chemistry and Function Manufacturing, and "the Belt and Road" International Joint Research Laboratory of Sustainable Materials, Southwest University, Chongqing 400715, People's Republic of China
e-mail: swucgl@swu.edu.cn

J. Huang
e-mail: huangjin2015@swu.edu.cn; huangjin@iccas.ac.cn

Y. Gong
College of Chemistry and Molecular Science, Wuhan University, Wuhan 430072, People's Republic of China

X. Li
Chengdu Banknote Printing Co., Ltd., Chengdu 611130, People's Republic of China

X. Jia · J. Huang
School of Chemistry and Chemical Engineering, and Engineering Research Center of Materials-Oriented Chemical Engineering of Xinjiang Bintuan, Shihezi University, Shihezi 832003, People's Republic of China

Published online: 17 January 2022

believe such cellulose-based materials can be widely used in optical sensors.

Keywords Cellulose nanocrystals · Poly(vinyl alcohol) · Uniaxial assembly · Mechanical responsiveness · Luminescence enhancement

Introduction

Periodic assembly structures with structural colors has great potential in optical sensors (Wu et al. 2019; Zhao et al. 2017), anti-counterfeiting (Chu et al. 2019), and information security (Yang et al. 2019). Unlike pigments or fluorescent materials, the structural color materials do not fade and are free of photo-bleaching (Echeverri et al. 2019; Wang et al. 2019; Zhang et al. 2019). The brightness and color of those assembly structures can also be adjusted via controlling their periodicity and orientation (Gu et al. 2016; Tong et al. 2016). Meanwhile, the uniaxial assembly membrane of rod-like cellulose nanocrystals (CNCs) was recently found to possess not only structural colors but also a property of assembly-induced emission (Gan et al. 2019). The length of CNCs could then be adjusted via choosing a suitable cellulosic resource, and then the optical information of the assembly membrane could hide in visible light.

However, the low toughness of CNC membranes from the low flexibility of CNCs has limited the application of their uniaxial assembly structure in optical sensors. Fortunately, CNCs could assemble in flexible matrices to enhance the mechanical properties of CNC membranes (Guidetti et al. 2016; Leng et al. 2018; Shopsowitz et al. 2012). Also, CNCs could self-assemble in the polymer precursors and form flexible hydrogel with structural colors after polymerization (Kelly et al. 2013; Khan et al. 2013). Those materials might further display different structural colors when stimulated by strain (Giese et al. 2013), humidity (Khan et al. 2015; Yao et al. 2017), and solvent (Giese et al. 2014), which gave CNC assemblies potential uses in sensors. For example, CNCs could be co-assembled with poly(ethylene glycol) (PEG), whose structural colors could be regulated by changing the fraction between CNCs and PEG, and the obtained films would respond to changes in humidity (Zhang et al. 2013). Besides, CNCs could assemble in phenol-formaldehyde resin, and then elastic membranes with structural colors that can make responses to strain and humidity were obtained via eliminating CNCs (Khan et al. 2013).

Although those studies showed that flexible CNC-based membranes could be used in optical sensors, their CNC assembly structures were chiral instead of uniaxial. The reason was related to the strong interaction between CNC particles, the main of which was hydrogen bonds (H-bonds). Thus, we co-assembled CNCs in poly(vinyl alcohol) (PVA), which could also form H-bonds and was flexible, and the assembly ratio between CNCs and PVA was controlled to obtain a uniaxial structure of CNCs. With a morphological test from atomic force microscopy, we found that the uniaxial assembly degree of the CNCs in PVA was even better than neat CNCs, leading to an increase in emission quantum efficiency from 13.90 to 61.10%. Then, the obtained PVA/CNC membranes showed wavelength shifts in emission and excitation under strain, along with a change in photoluminescent intensity, which could be directly observed by naked eyes. The mechanism study in such a stimulation-response phenomenon suggested that the response mainly came from the change in the effective refractive index of the membrane, and the assembly ratio between CNCs and PVA played a key role in increasing response sensitivity. Since the PVA/CNC co-assembly structure possessed high quantum-efficiency and flexibility, it could not only be applied in the optical sensor, but also in the field of information security, like anti-counterfeiting labels and invisible patterns.

Experimental sections

Materials

Cotton linter was obtained from Hubei Chemical Fiber Group Co., Ltd. (China). Poly(vinyl alcohol) (PVA, 1788 model with the alcoholysis degree of 87.0 ~ 89.0%) was purchased from Greagent (China), and sodium hydroxide (NaOH) and sulfuric acid (H_2SO_4, 98%) were purchased from Aladdin (China).

Extraction of cellulose nanocrystals (CNCs)

CNCs were extracted from cotton linters by acid hydrolysis with H_2SO_4 according to the previous work (Li et al. 2019). For the first step, the linters were treated with a 2 wt% NaOH solution (generally 50 g fibers for 2 L solution) for 12 h at room temperature. Then the alkali-treated fiber was filtered and washed with distilled water for about 3 times to get a neutral supernatant. After that, the acid hydrolysis (12.5 g fiber for 250 mL solution) was conducted at 45 °C using 65 wt% H_2SO_4 with mechanical stirring for 60 min. Subsequently, the suspension was quenched by diluting with about 600 mL cold deionized water, washed several times, and centrifuged at a rotation rate of 4000 rpm. Subsequently, the suspension was dialyzed until neutrality. Finally, a high concentration (3 wt%) of the CNC suspension was obtained by rotary evaporation.

Preparation of the CNC/PVA uniaxial co-assembled membranes

Firstly, 20 g of PVA was dissolved into 180 g deionized water under mechanical stirring at 95 °C for about 2 h to prepare an aqueous solution of 10 wt% PVA. Subsequently, the given amount of CNC suspension was added into the PVA solution with magnetic stirring to gain a homogeneous suspension. After short sonication, 10 mL mixture suspension was poured into a 30 mL sample bottle, and a sliding glass was vertically inserted into the suspension, then the CNC/PVA membranes were obtained by evaporating the water at 30 °C. Based on the mass ratio of CNCs and PVA in the resultant membrane, the samples were coded as CNC-X, where the number X represented the mass percentage of CNCs in the total of CNCs and PVA.

Characterizations

Ultraviolet and visual adsorption (UV–vis), zeta potential, photoluminescence (PL) spectra, and PL emission quantum yield analysis

UV–vis tests were carried out on a Cary Lambda 750 S spectrophotometer (PerkinElmer). Zeta potential of CNC/PVA suspension (pH = 7) was measured by a NanoBrook Omni (Brookhaven). PL spectra of CNC/PVA membranes were tested on the 5JI-004 (Hitachi) with the solid-state mode. The measurement of PL emission quantum efficiency (EQE) was conducted with F-4500 fluorescence spectrophotometer (Hitachi). The measuring conduction was the solid-state mode.

Scanning electron microscopy (SEM) and atomic force microscope (AFM)

The fracture plane morphologies of the CNC/PVA assembly membranes were characterized by SEM using a JSM-IT300 field emission scanning electron microscope (JEOL), and the acceleration voltage was 10.0 kV. The morphologies of the membranes were carried on a Dimension Icon (Bruker). The characterizations were tested by the tip of Scanasyst-air under the Scanasyst mode and by the tip of OTESPA-R3 under the Tapping mode.

Tensile tests

Tensile tests were performed using a CMT6503 universal testing machine (SANS) with a strain rate of tensile tests at 5 mm/min. For CNC-50 and CNC-40 membranes, they were strengthened to an elongation of 20%, 40%, 60%, 80% and till broke to make the PL tests.

Thermogravimetric analysis (TGA)

TGA tests were performed using TGA 4000 (PerkinElmer). The experiments were tested under dry nitrogen purge at a flow rate of 10 mL/min from room temperature to 800 °C at the heating rate of 40 °C/min.

X-ray diffraction (XRD)

XRD was used to study the structural property of CNC/PVA co-assembly membranes before and after stretching, and it was carried out on X-Ray diffractometer (XRD-6000; Shimadzu, Japan). Cu Kα radiation was operated at $\lambda = 0.154$ nm from 5 to 50° with a step speed of 2°/min.

Results and discussions

Luminescence properties and mechanical response of CNC/PVA co-assembly membranes

Stable dispersion of cellulose nanocrystals (CNCs) in suspension is necessary for the uniaxial assembly of CNCs. Table 1 shows the zeta-potential of CNCs in the suspension with poly(vinyl alcohol) (PVA) with different ratios, which indicated that neat CNC suspension possessed an extremely high zeta potential of −72.2 mV. As the PVA percentage increased, the zeta potential decreased but remained at a high level of > 30 mV, which indicated the suspensions were still highly stable (Kiprono et al. 2018). In order to eliminate the chiral structure, the zeta potential of the CNC dispersion should not be too high to achieve the uniaxial assembly with higher orientation. Thus, the CNC/PVA system should has a better assembly potential than neat CNCs.

Figure 1a shows the absorption spectra of CNC/PVA co-assembled membranes. Since both cellulose and PVA had no absorption in UV and visible range, the absorption peaks around 368 nm must come from the structural colors of the CNC assembly. The photoluminescence (PL) spectra in Fig. 1b show excitation peaks at similar wavelengths and the excitation (Ex) wavelengths were around 368 nm. Those results suggested that CNCs could uniaxially assemble with PVA and emit blue light under UV light.

Figure 2a, b proved the uniaxial assembly structure still existed in the CNC/PVA composites, but PVA took up a large volume, and it wrapped CNCs around it. As seen in Fig. 2c, d, for the fracture surfaces of CNC-50 and CNC-40 displayed similar results, there were no apparent chiral structures, and they were both smooth. However, in Fig. 2e, CNC-100 showed a different format under the larger observation size than CNC-40 and CNC-50. It could be the large scale of chiral nematic structure though it had a high orientation in small size less than 1 μm. This was also the reason for the EQE of the CNC/PVA uniaxial co-assembly composites were much higher than that of the neat CNC membrane.

The percentage of CNCs also affected the mechanical and tensile-response properties of the CNC/PVA membranes. CNC-80 and CNC-60 showed a low elongation at break, which was 4.2% and 7.0%, respectively, when that of neat CNC membranes were less than 0.1%. Those membranes displayed no tensile responsiveness. By contrast, the elongation at the break of CNC-50, CNC-40, and CNC-20 could be more than 90%. Furthermore, CNC-50 and CNC-40 exhibited shifts in excitation (Ex) wavelengths during stretching, while CNC-20 showed little responsiveness. In detail, the Ex wavelength of CNC-50 showed an apparent blue shift when the elongation reached 40%, and it continued to decrease to 346 nm at the break, compared with the initial Ex wavelength of 368 nm, as shown in Fig. 3. The Ex wavelength of CNC-40 samples displayed similar results, and the maximal decrement of Ex wavelengths was 22 nm and 17 nm for CNC-50 and CNC-40, respectively. Emission (Em) wavelengths of CNC-50 and CNC-40 also showed a slight blue shift overall when the elongation increased from 0 to 90% and from 0 to 94%, respectively.

Besides, the luminesce intensity also increased during the stretching. As shown in Table 2, the emission quantum efficiency (EQE) of CNC-50 and CNC-40 were 48.30% and 60.60%, respectively, both of which were much higher than neat CNC uniaxial assembly membranes (13.90%) (Gan et al. 2019). During stretching, the EQE of CNC-50 and CNC-40 increased to 61.10% and 63.52%, respectively, and their photoluminescent lifetime also increased slightly. Figure 4 also illustrates that the luminous intensity of CNC/PVA membranes was higher after tensile treatment.

Table 1 Zeta potential values of CNC/PVA suspension

Samples	CNC-100	CNC-80	CNC-60	CNC-50	CNC-40	CNC-20
Zeta Potential (mV)	−72.2	−46.5	−44.3	−43.5	−42.2	−38.9

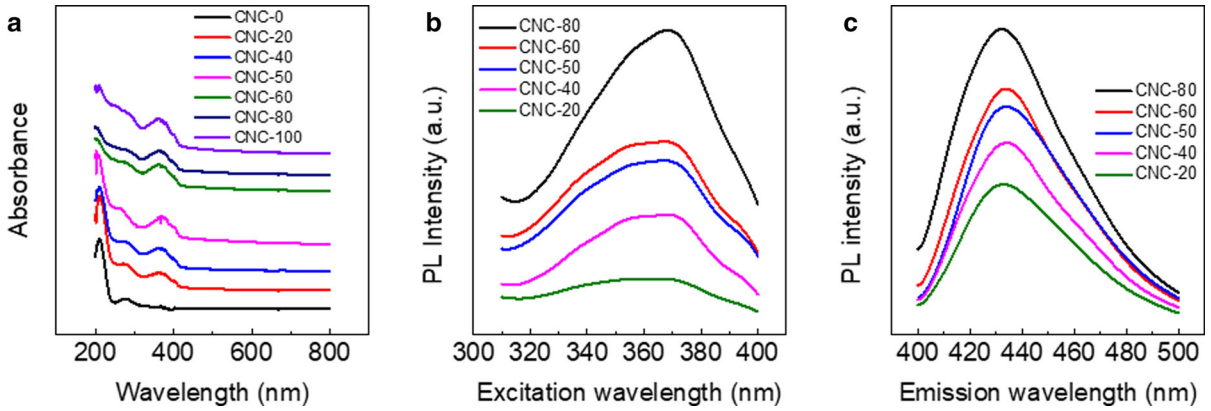

Fig. 1 **a** UV–vis spectra, **b** excitation and **c** emission spectra of CNC/PVA samples with different CNC content

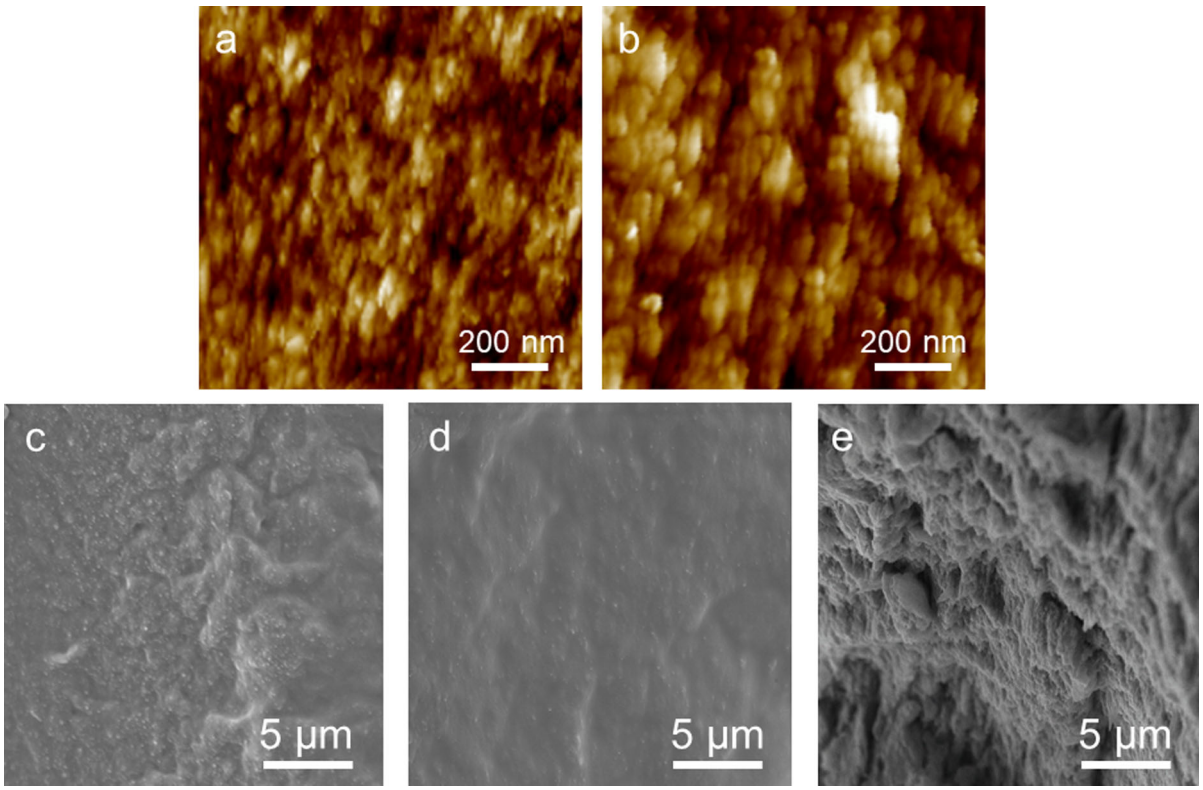

Fig. 2 AFM images of **a** CNC-50 and **b** CNC-40, and fracture surfaces SEM images of **c** CNC-50, **d** CNC-40, and **e** CNC-100

Responsiveness mechanism

The mechanisms of tensile response and photoluminescent enhancement were studied with the uniaxial assembly structure of CNCs as the beginnings shown in Scheme 1. The CNC assembly was regarded as a dense hexagonal arrangement (DHA) in the PVA matrix (Wang and Walther 2015), and the Bragg-diffraction wavelength (λ) of the uniaxially assembled CNCs could be expressed by Eq. (1) (Gan et al. 2019):

$$m\lambda = 2D\sqrt{n_{\text{eff}}^2 - \sin^2\theta} \tag{1}$$

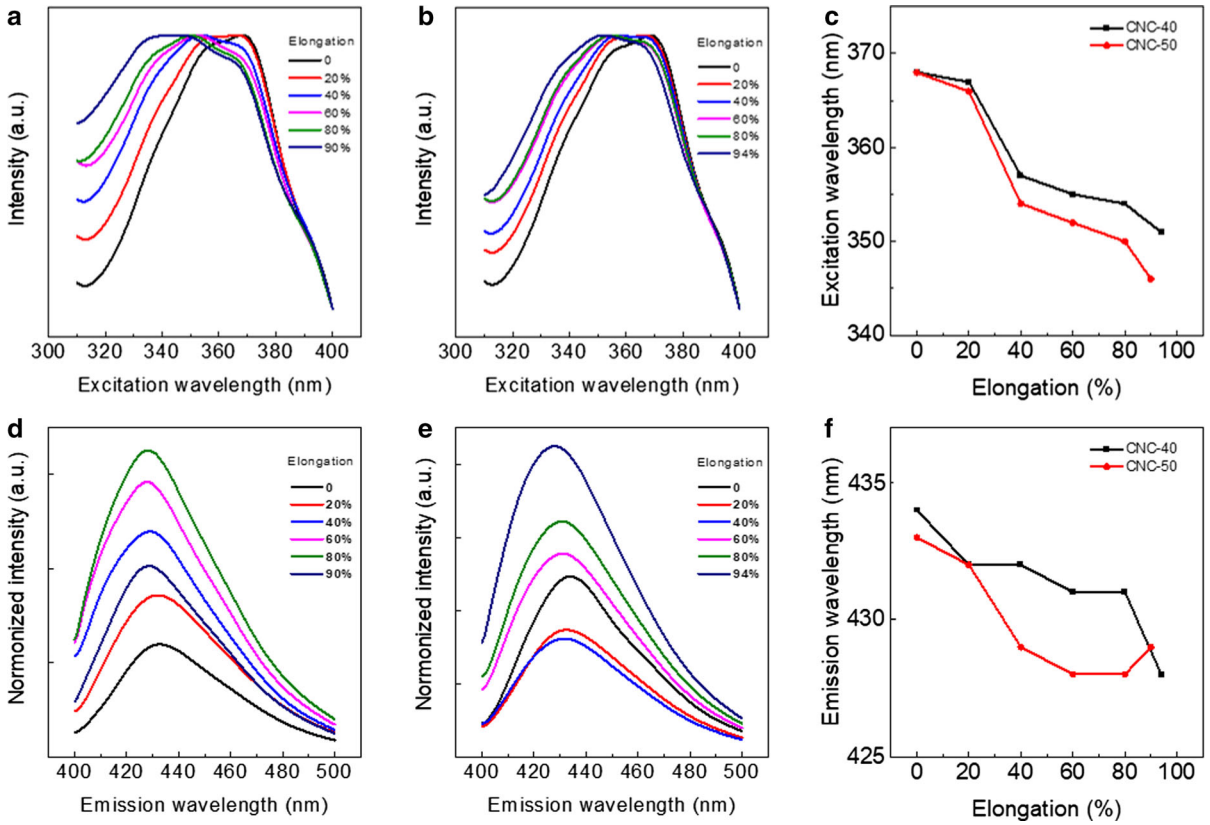

Fig. 3 Intensity of excitation spectra for **a** CNC-50 and **b** CNC-40, emission spectra for **d** CNC-50 and **e** CNC-40 at different elongations; **c** and **f** line chart of excitation wavelengths and emission wavelength along with elongations for CNC-50 and CNC-40

Table 2 EQE of CNC-50 and CNC-40 before and after stretching

Samples	Lifetime (ns)	EQE (%)
CNC-40	1.26	48.30
CNC-40 at 80% elongation	1.27	61.11
CNC-50	1.18	60.60
CNC-50 at 80% elongation	1.22	63.52

where m is the diffraction order. For CNCs, the m should be 1 (Gan et al. 2019). n_{eff} is the effective refractive index, D is the vertical periodicity, and θ is the incident angle.

In this work, the incident angle was 90°, thus the value of $\sin^2\theta$ was 1. The refractive index of CNCs and PVA were 1.534 (Shopsowitz et al. 2010) and 1.520–1.550 (Natarajan and Gilman 2017), respectively. Since the λ was 368 nm, the D should be

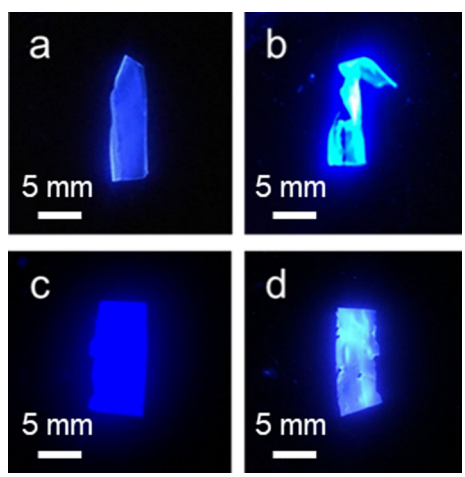

Fig. 4 **a** CNC-50, **c** CNC-40 membrane and **b** CNC-50, **d** CNC-40 membrane after stretching under 365 nm UV light

158.2 nm, which was slightly larger than the average length of CNCs. The difference should be ascribed to the introduction of PVA between CNCs.

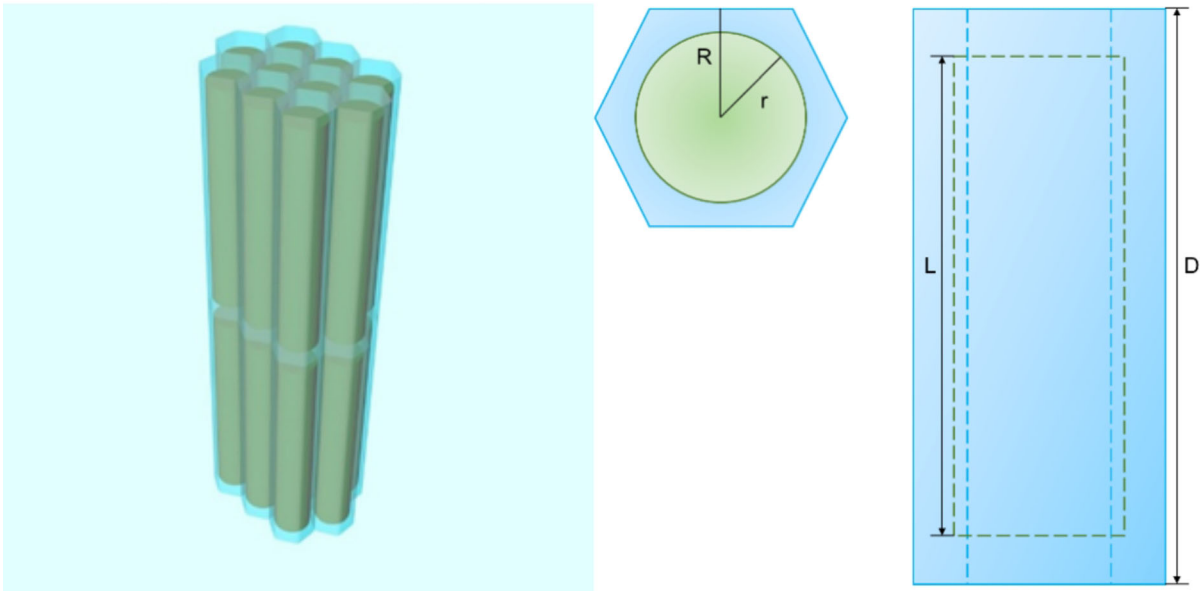

Scheme 1 Schematic diagram of the assembled structure of CNC/PVA materials

After stretching, the Ex wavelength of both CNC-40 and CNC-50 firstly decreased a little at the elongation of 20%, and then showed a substantial decrement as the elongation increased from 20 to 40%, then steeply decrease until the break. The decrease of Ex wavelength might be from the change in D and n_{eff}. However, we found the change was mainly attributed to the n_{eff}. The n_{eff} decreased with an increasing strain due to the vacuum, which resulted in a lower refractive index. The length of CNCs were 144 ± 26 nm and radius were 9.0 ± 1.2 nm according to the AFM image Fig. 5. In byte DHA of CNCs in PVA, we regarded CNC as a cylinder with a radius of r (4.5 nm), a length of L (144 nm), and a minimum vertical distance between CNC particles of e. The edge of hexagonal was coded as R. According to the thermogravimetry analysis (TGA) results in Table 3, the CNC component of CNC-50 and CNC-40 was calculated to be 64.5 wt% and 43.7 wt%, respectively, with Eq. (2) (Liu et al. 2019):

$$C = \frac{W_{\text{CNC/PVA}} - W_{\text{PVA}}}{W_{\text{CNC}} - W_{\text{PVA}}} \times 100\% \tag{2}$$

where $W_{\text{CNC/PVA}}$, W_{CNC}, and W_{PVA} were the residual weight of CNC/PVA, CNCs, and PVA at 800 °C, respectively. With the densities of CNCs and PVA (1.56 g cm^{-3} (Giese et al. 2015) and 1.19 g cm^{-3} (Wang and Walther 2015), respectively), the volume fraction (V_{CNC}) of CNC-50 and CNC-40 should be 58.1% and 37.2%, thus R could be calculated by Eq. (3):

$$R = \sqrt{\frac{\pi r^2 L}{2\sqrt{3} D \times V_{\text{CNC}}}} \tag{3}$$

The R of CNC-50 and CNC-40 were 5.36 nm and 6.70 nm, respectively, which indicated CNCs might be tightly arranged in the PVA matrix. We first assumed the D changed, which meant it must decrease during stretching to keep consistency with the

Table 3 Residual weight of different CNC/PVA membranes at 800 °C

Samples	CNC-100	CNC-50	CNC-40	CNC-20	CNC-0
Residual weight (wt%)	26.02	17.13	11.92	4.76	1.03
CNC content (wt%)	100.0	64.5	43.7	15.0	0.0

decrease in λ. However, the decreasing D implied the material was shrinking, which was clearly contradicted to the tensile test conditions.

Then, we assumed the D was constant and the n_{eff} decreased during stretching due to the vacuum generation, thus we could calculate the n_{eff} of stretched membranes with Eq. (4) (Zhao et al. 2012):

$$n_{\text{eff}}^2 = n_1^2 f_1 + n_2^2 f_2 \tag{4}$$

where n_1 and n_2 are the effective refractive index of PVA/CNC and vacuum, the value of n_2 is 1, and f_2 is the fraction of vacuum and air. Apparently, $f_2 = 1 - f_1$.

The results of f_1 were shown in Table 4. The Δf_1 displayed the same tendency of the change by stretching the CNC-50 and CNC-40 membranes. Those results suggested that the membranes did not gain much vacuum or air at first, thus the λ nearly did not change when the elongation was smaller than 20%. By contrast, when the elongation increased further, the plastic strain of PVA led to the introduction of vacuum and air. Then the f_2 increased rapidly, and thus the Ex decreased obviously. Subsequently, with stationary stretching, the vacuum generation of CNC-50 and CNC-40 showed consistent results of Δf_1 with the change of elongation. Finally, the materials fractured and resulted in a massive change in n_{eff}, which led to a large decrease in Ex wavelength again.

The results were also coincident with SEM and XRD analysis. Compared with the unscratched membrane in Fig. 2c, the stretched membrane in Fig. 6a seemed to possess better orientation, and the traces of vacuum during stretch could be found. Meanwhile, the CNC-40 fracture surfaces displayed similar results, but the orientation was not noticeable. The XRD results in Fig. 7a, b displayed a typical diffraction peak at 2θ values of around 22.0° in all samples, which

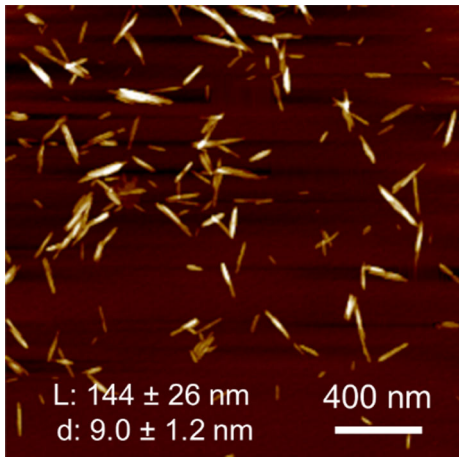

Fig. 5 AFM image of CNCs prepared by 10 μL 0.001 wt% dispersion

is coincident with diffraction planes of (200) in the cellulose I crystal (French 2014). The diffraction peak at 2θ values of around 20° belongs to the PVA (Kim et al. 2020). The crystallinity of CNCs can be represented by Segal crystallinity index (CrI) (French and Santiago Cintrón 2013). CrI of CNC-40 and CNC-50 decreased from 73.73 to 58.86% and from 79.25 to 64.77%, respectively after stretching, which resulted from the decrease of relative density of CNCs under the same scan area. On the other hand, the photoluminescence of CNC/PVA co-assembly membranes came from the improved virtual transition of the uniaxial assembly CNCs (Gan et al. 2019). The uniaxial orientation degree of CNCs further improved after stretching, resulting in the enhancement of virtual transition. Thus, the EQE showed a lift after stretching. In addition, although CNC-20 was also tough, the CNC content was too low (15.0 wt%). Thus, the formation of the vacuum could be hard, and it

Table 4 λ, n_{eff}, f_1, and Δf_1 at different elongation for CNC-50 and CNC-40

CNC-50					CNC-40				
Elongation (%)	λ (nm)	n_{eff}	f_1	Δf_1	Elongation(%)	λ (nm)	n_{eff}	f_1	Δf_1
20	366	1.529	0.989	–	20	367	1.531	0.994	–
40	354	1.500	0.926	0.063	40	357	1.508	0.941	0.053
60	352	1.496	0.915	0.011	60	355	1.503	0.931	0.010
80	350	1.491	0.909	0.006	80	354	1.500	0.926	0.005
90	346	1.482	0.884	0.023	94	351	1.494	0.910	0.016

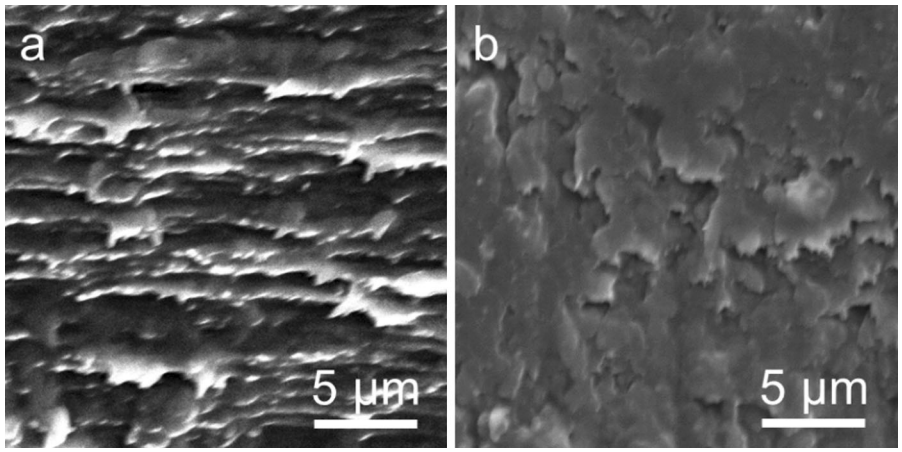

Fig. 6 Fracture surfaces SEM images of stretched **a** CNC-50 and **b** CNC-40

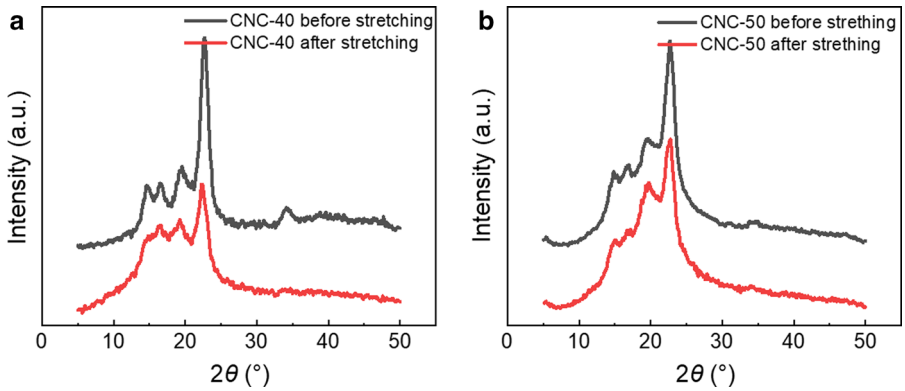

Fig. 7 XRD pattern of **a** CNC-40 and **b** CNC-50 before and after stretching

showed little response to mechanical stimulation. These results also confirmed our assumption that the decrease of the Ex wavelength and the luminescence enhancement of CNC/PVA membrane resulted from the change in n_{eff} should be correct.

Conclusions

Cellulose nanocrystals (CNCs) were able to assemble uniaxially to form photoluminescent membranes, but the brittleness of the material limited the application. Herein, we combined the advantages of flexible poly(vinyl alcohol) (PVA) and assembled abilities of CNCs to co-assemble uniaxially to form flexible photoluminescent membranes. In addition, we regulated the mass fraction of the two components to control the tensile property and luminesce intensity of the co-assembled membranes. The obtained composites had not only high photoluminescence quantum yields (EQE), but also gained mechanical response capacity. With the introduction of PVA, the elongation at break of the material increased to more than 90%, and the excitation (Ex) wavelength decreased with the increase of the elongation. In addition, the EQE increased a lot compared with the neat CNC membrane, and it further increased after stretching. We studied the mechanism of such responsiveness and constructed a close-packed hexagonal model of the CNC assembly. Through the calculating, we found the decrease of Ex wavelengths was attributed to the formation of vacuum during the tensile treatment. The vacuum could change the effective refractive index (n_{eff}) and thus cause a decrease of the Bragg-diffraction wavelengths. Too little PVA in CNC/PVA composites could lead to brittle materials, while too

much might result in a loss of responsiveness. The CNC/PVA membranes possessed a much higher emission intensity for the elimination of chiral structure and showed mechanical responses. Thus, the flexible photoluminescent materials have the potential in anti-counterfeiting and mechanical sensing fields.

Acknowledgments This research is financially supported by the National Natural Science Foundation of China (51603171 and 51973175), the Project for Chongqing University Innovation Research Group (CXQT19008), the Chongqing Talent Plan for Innovation and Entrepreneurship Demonstration Team (CQYC201903243), and the Technological Innovation and Application Development "Overall Rationing System" Project of Chongqing Talent Plan (CSTC2021YCJH-BGZXM0307).

Declarations

Conflict of interest The authors declare no competing financial interest.

References

Chu L, Zhang X, Niu W, Wu S, Ma W, Tang B, Zhang S (2019) Hollow silica opals/cellulose acetate nanocomposite films with structural colors for anti-counterfeiting of banknotes. J Mater Chem C 7:7411–7417. https://doi.org/10.1039/c9tc01992h

Echeverri M, Patil A, Xiao M, Li W, Shawkey MD, Dhinojwala A (2019) Developing noniridescent structural color on flexible substrates with high bending resistance. ACS Appl Mater Inter 11:21159–21165. https://doi.org/10.1021/acsami.9b04560

French AD (2014) Idealized powder diffraction patterns for cellulose polymorphs. Cellulose 21:885–896. https://doi.org/10.1007/s10570-013-0030-4

French AD, Cintron MS (2013) Cellulose polymorphy, crystallite size, and the Segal crystallinity index. Cellulose 20:583–588. https://doi.org/10.1007/s10570-012-9833-y

Gan L, Feng N, Liu S, Zheng S, Li Z, Huang J (2019) Assembly-induced emission of cellulose nanocrystals for hiding information. Part Part Syst Char 36:1800412. https://doi.org/10.1002/ppsc.201800412

Giese M, Blusch LK, Khan MK, Hamad WY, MacLachlan MJ (2014) Responsive mesoporous photonic cellulose films by supramolecular cotemplating. Angew Chem Int Edit 53:8880–8884. https://doi.org/10.1002/anie.201402214

Giese M, Blusch LK, Khan MK, MacLachlan MJ (2015) Functional materials from cellulose-derived liquid-crystal templates. Angew Chem Int Edit 54:2888–2910. https://doi.org/10.1002/anie.201407141

Giese M, Khan MK, Hamad WY, MacLachlan MJ (2013) Imprinting of photonic patterns with thermosetting amino-formaldehyde-cellulose composites. ACS Macro Lett 2:818–821. https://doi.org/10.1021/mz4003722

Gu M, Jiang C, Liu D, Prempeh N, Smalyukh II (2016) Cellulose nanocrystal/poly(ethylene glycol) composite as an iridescent coating on polymer substrates: structure-color and interface adhesion. ACS Appl Mater Inter 8:32565–32573. https://doi.org/10.1021/acsami.6b12044

Guidetti G, Atifi S, Vignolini S, Hamad WY (2016) Flexible photonic cellulose nanocrystal films. Adv Mater 28:10042–10047. https://doi.org/10.1002/adma.201603386

Kelly JA, Shukaliak AM, Cheung CC, Shopsowitz KE, Hamad WY, MacLachlan MJ (2013) Responsive photonic hydrogels based on nanocrystalline cellulose. Angew Chem Int Edit 52:8912–8916. https://doi.org/10.1002/anie.201302687

Khan MK, Bsoul A, Walus K, Hamad WY, MacLachlan MJ (2015) Photonic patterns printed in chiral nematic mesoporous resins. Angew Chem Int Edit 54:4304–4308. https://doi.org/10.1002/anie.201410411

Khan MK, Giese M, Yu M, Kelly JA, Hamad WY, MacLachlan MJ (2013) Flexible mesoporous photonic resins with tunable chiral nematic structures. Angew Chem Int Edit 52:8921–8924. https://doi.org/10.1002/anie.201303829

Kim J, Jayaramudu T, Zhai LD, Kim HC, Agumba DO (2020) Preparation of cellulose nanocrystal-reinforced physical hydrogels for actuator application. Curr Comput-Aided Drug Des 10:969. https://doi.org/10.3390/cryst10110969

Kiprono SJ, Ullah MW, Yang G (2018) Encapsulation of E. coli in biomimetic and Fe_3O_4-doped hydrogel: structural and viability analyses. Appl Microbiol Biot 102:933–944. https://doi.org/10.1007/s00253-017-8625-6

Leng JX, Li GH, Ji XX, Yuan ZW, Fu YJ, Li HG, Qin MH, Moehwald H (2018) Flexible latex photonic films with tunable structural colors templated by cellulose nanocrystals. J Mater Chem C 6:2396–2406. https://doi.org/10.1039/c7tc05523d

Li D, Wang Y, Long F, Gan L, Huang J (2019) Solvation-controlled elastification and shape-recovery of cellulose nanocrystal-based aerogels. ACS Appl Mater Inter 12:1549–1557. https://doi.org/10.1021/acsami.9b18569

Liu S, Chen Y, Liu C, Gan L, Ma X, Huang J (2019) Polydopamine-coated cellulose nanocrystals as an active ingredient in poly(vinyl alcohol) films towards intensifying packaging application potential. Cellulose 26:9599–9612. https://doi.org/10.1007/s10570-019-02749-7

Natarajan B, Gilman JW (2017) Bioinspired Bouligand cellulose nanocrystal composites: a review of mechanical properties. Philos T R Soc A 376:20170050. https://doi.org/10.1098/rsta.2017.0050

Shopsowitz KE, Hamad WY, MacLachlan MJ (2012) Flexible and iridescent chiral nematic mesoporous organosilica films. J Am Chem Soc 134:867–870. https://doi.org/10.1021/ja210355v

Shopsowitz KE, Qi H, Hamad WY, MacLachlan MJ (2010) Free-standing mesoporous silica films with tunable chiral nematic structures. Nature 468:422–425. https://doi.org/10.1038/nature09540

Tong L, Qi W, Wang M, Huang R, Su R, He Z (2016) Tunable design of structural colors produced by pseudo-1d photonic crystals of graphene oxide. Small 12:3433–3443. https://doi.org/10.1002/smll.201600148

Wang B, Walther A (2015) Self-assembled, iridescent, crustacean-mimetic nanocomposites with tailored periodicity and layered cuticular structure. ACS Nano 9:10637–10646. https://doi.org/10.1021/acsnano.5b05074

Wang F, Feng L, Qin Y, Zhao T, Luo H, Zhu J (2019) Dual functional SiO_2@TiO_2 photonic crystals for dazzling structural colors and enhanced photocatalytic activity. J Mater Chem C 7:11972–11983. https://doi.org/10.1039/c9tc03426a

Wu J, Niu W, Zhang S, Wu S, Ma W, Tang B (2019) A flexible and robust dual-network supramolecular elastic film with solvent resistance and brilliant structural colors. New J Chem 43:11517–11523. https://doi.org/10.1039/c9nj02308a

Yang D, Liao G, Huang S (2019) Invisible photonic prints shown by UV illumination: combining photoluminescent and noniridescent structural colors. J Mater Chem C 7:11776–11782. https://doi.org/10.1039/c9tc03982a

Yao K, Meng Q, Bulone V, Zhou Q (2017) Flexible and responsive chiral nematic cellulose nanocrystal/poly (ethylene glycol) composite films with uniform and tunable structural color. Adv Mater 29:1701323. https://doi.org/10.1002/adma.201701323

Zhang J, Zhu Z, Yu Z, Ling L, Wang C-F, Chen S (2019) Large-scale colloidal films with robust structural colors. Mater Horiz 6:90–96. https://doi.org/10.1039/c8mh00248g

Zhang YP, Chodavarapu VP, Kirk AG, Andrews MP (2013) Structured color humidity indicator from reversible pitch tuning in self-assembled nanocrystalline cellulose films. Sensor Actuat B-Chem 176:692–697. https://doi.org/10.1016/j.snb.2012.09.100

Zhao Y, Xie Z, Gu H, Zhu C, Gu Z (2012) Bio-inspired variable structural color materials. Chem Soc Rev 41:3297. https://doi.org/10.1039/c2cs15267c

Zhao Z, Wang H, Shang L, Yu Y, Fu F, Zhao Y, Gu Z (2017) Bioinspired heterogeneous structural color stripes from capillaries. Adv Mater 29:1704569. https://doi.org/10.1002/adma.201704569